Neurobiology of Disease 156 (2021) 105420

Contents lists available at ScienceDirect

Neurobiology of Disease

journal homepage: www.elsevier.com/locate/ynbdi

Super-resolution STED microscopy in live brain tissue

Stefano Calovi [a,b,c], Federico N. Soria [c,d], Jan Tønnesen [c,d,*]

[a] Laboratory of Molecular Pharmacology, Institute of Experimental Medicine, Budapest, Hungary
[b] János Szentágothai Doctoral School, Semmelweis University, Budapest, Hungary
[c] Achucarro Basque Center for Neuroscience, Leioa, Spain
[d] Department of Neuroscience, Faculty of Medicine and Nursing, University of the Basque Country (UPV/EHU), Leioa, Spain

ARTICLE INFO

Keywords:
STED microscopy
Super-resolution
Live imaging
Synapses
Dendritic spines
Brain extracellular space

ABSTRACT

STED microscopy is one of several fluorescence microscopy techniques that permit imaging at higher spatial resolution than what the diffraction-limit of light dictates. STED imaging is unique among these super-resolution modalities in being a beam-scanning microscopy technique based on confocal or 2-photon imaging, which provides the advantage of superior optical sectioning in thick samples. Compared to the other super-resolution techniques that are based on widefield microscopy, this makes STED particularly suited for imaging inside live brain tissue, such as in slices or *in vivo*. Notably, the 50 nm resolution provided by STED microscopy enables analysis of neural morphologies that conventional confocal and 2-photon microscopy approaches cannot resolve, including all-important synaptic structures. Over the course of the last 20 years, STED microscopy has undergone extensive developments towards ever more versatile use, and has facilitated remarkable neurophysiological discoveries.

The technique is still not widely adopted for live tissue imaging, even though one of its particular strengths is exactly in resolving the nanoscale dynamics of synaptic structures in brain tissue, as well as in addressing the complex morphologies of glial cells, and revealing the intricate structure of the brain extracellular space. Not least, live tissue STED microscopy has so far hardly been applied in settings of pathophysiology, though also here it shows great promise for providing new insights.

This review outlines the technical advantages of STED microscopy for imaging in live brain tissue, and highlights key neurobiological findings brought about by the technique.

1. Surpassing the resolution limit in fluorescence microscopy

The field of super-resolution fluorescence microscopy has flourished and diversified extensively since its budding from the fluorescence microscopy tree more than 20 years ago (Hell and Wichmann, 1994). The fundamental principle behind fluorescence microscopy is the use of excitation light of one wavelength to bring fluorophores into an excited energy state, from where they emit fluorescence at a different wavelength, allowing spectral separation and observation of fluorescence at high contrast on a dark background. The common denominator of the super-resolution techniques is the control of the energy states of fluorophore populations over space and time, to constrict when and where these emit fluorescence. Current modalities that qualify as such techniques can be categorized broadly into two groups: 1) single-molecule localization microscopy (SMLM) approaches, represented by the main incarnations stochastic optical reconstruction microscopy (STORM) (Rust et al., 2006) and photoactivated localization microscopy (PALM) (Betzig et al., 2006; Hess et al., 2006); and 2) coordinate-targeted imaging approaches that rely on patterned illumination modalities, including neuroscience household names structured illumination microscopy (SIM) (Gustafsson, 2000, 2005), and stimulated emission depletion (STED) microscopy (Klar et al., 2000).

Even though expansion microscopy can be considered a super-resolution technique, it works by chemically processing the sample to volumetrically expand it, thus increasing the physical distance between molecules and allowing otherwise irresolvable sample structures to be optically resolved in a conventional microscope. It is therefore in essence a sample preparation technique, rather than a microscopy approach (Chen et al., 2015).

Members of the SMLM family collect images by consecutively acquiring frames of subsets of stochastically activated fluorophores from a given labeled sample, computing the corresponding fluorophore

* Corresponding author at: Achucarro Basque Center for Neuroscience, Leioa, Spain.
E-mail address: jan.tonnesen@ehu.eus (J. Tønnesen).

https://doi.org/10.1016/j.nbd.2021.105420
Received 31 December 2020; Received in revised form 3 June 2021; Accepted 4 June 2021
Available online 5 June 2021
0969-9961/© 2021 The Authors. Published by Elsevier Inc. This is an open access article under the CC BY-NC-ND license (http://creativecommons.org/licenses/by-nc-nd/4.0/).

center location maps, and merging these into a final image. They rely on individual non-overlapping fluorescent emitters being discernible within a given frame, in order for their center positions to be mathematically pinpointed to a sub-diffraction 2D area or 3D volume, as recently reviewed (Möckl and Moerner, 2020). Once a sufficient number of fluorophore position maps have been collected, their sum will describe the underlying labeled structure. This fluorophore mapping approach generally achieves better spatial resolution than the patterned illumination approaches, and allows routine imaging at around 20 nm resolution (Khater et al., 2020). The MINFLUX technique has impressively achieved around 2 nm resolution by combining principles of SMLM and patterned illumination microscopy (Gwosch et al., 2020). A prerequisite for the SMLM approach is that indeed the sample is covered by fluorophores at sufficient density for these to adequately report the underlying structure, which is especially true for immobile fluorophores, *i.e.* when imaging immunochemically labeled fixed samples (Dempsey et al., 2011). In addition to creating structural images, SMLM allows tracking of moving single particles across frames, *e.g.* to track individual labeled proteins diffusing in the cell membrane (Manley et al., 2008).

Single emitter discrimination is not a concern for the patterned illumination approaches, and these are particularly suited for *ensemble imaging* of dense populations of fluorophores that are imaged collectively, including cytosolic or membrane bound freely diffusing fluorophores. In the context of this review, it is worth highlighting that SIM can be applied as either saturated or non-saturated SIM, where *saturation* refers to the excitation state of the involved fluorophore population. In saturated SIM, higher excitation powers are used to drive fluorophores into the excited state until this population starts to saturate, so that emission intensity no longer scales linearly with excitation intensity, hence it is also referred to as non-linear SIM (Gustafsson, 2005). Saturated SIM can readily bypass the diffraction barrier and theoretically achieve unlimited resolution, though the required excitation powers become limiting, as they are associated with irreversible photobleaching of the fluorophores and putative phototoxicity in live cell imaging. On the other hand, linear SIM does not rely on saturating the excited state (Gustafsson, 2000), and utilizes excitation powers that are readily compatible with time-lapse live cell imaging without photobleaching or toxicity (Kner et al., 2009). Regular (non-saturated) linear SIM is thus more widely applied, though it can maximally enhance imaging resolution by a factor of two, similar to what can be achieved in confocal microscopy by decreasing the confocality pinhole aperture (Centonze and Pawley, 1995). Because linear SIM is still diffraction-limited, we will not include it in our further discussion among the super-resolution approaches.

STED microscopy also relies on introducing a non-linearity in the interaction between light and fluorophore populations, though here the saturation is not of the excited state, but the *depletion* of the excited state with the aim of preventing spontaneous fluorescence. While it is difficult to compare STED and saturated SIM because they differ so fundamentally, the general strategy of not aggressively forcing fluorophores into the excited state conceivably makes STED less prone to photobleaching and -toxicity than saturated SIM, because the excited state is more susceptible to unwanted transitions than the ground state (Icha et al., 2017). We describe in basic terms the principles of STED microscopy further below, and for a review on the working principles behind the remaining super-resolution modalities and a comparison of their main features we refer to designated reviews (Tønnesen and Nagerl, 2013; Schermelleh et al., 2019).

Light-sheet, or single plane illumination, microscopy excites the labeled sample with a thin sheet of light and thus produces very good optical sectioning when collecting the image through a microscope objective positioned perpendicularly to the illumination plane (Huisken et al., 2004). It is a highly versatile approach that is applicable for both diffraction-limited and super-resolution microscopy configurations, with the limiting factor for super-resolution imaging being the integrity of the light-sheet as imaging depth increases, as recently reviewed (Power and Huisken, 2017). Light-sheet microscopy allows both 3D SMLM and patterned illumination super-resolution microscopy (Lu et al., 2019), and especially lattice light-sheet microscopy offers spectacular spatiotemporal resolution at very low illumination intensities, allowing large volume extended time-lapse imaging of living cells without photobleaching or –toxicity (Chen et al., 2014). The standard light-sheet imaging configuration of two orthogonal microscope objectives limits its practicability for live cell imaging in tissue and *in vivo*. However, more recently, simpler single objective configurations have been introduced, including STORM based on oblique-plane light-sheet illumination that allowed imaging down to 60 μm tissue depth in fixed samples (Kim et al., 2019). It will be very interesting to follow further development along these lines, in particular from a live tissue perspective.

Each of the super-resolution modalities comes with practical advantages and shortcomings regarding the type of sample they are suited for and the type of imaging data they provide. Compared to the SMLM approaches, STED microscopy will nearly always fall short in terms of achievable resolution and photon burden in terms of required light intensities to acquire an image. This is a considerable drawback, because of the elevated risk of photobleaching and phototoxicity in settings of live cell imaging. Designated efforts are being invested in further reducing the photons required to acquire a given STED microscopy image (Jahr et al., 2020). STED has historically been associated with higher technical complexity and commercial price, though also on this front the differences are gradually evening out, as commercial plug-and-play options become increasingly available.

STED microscopy holds a key advantage in the ability to optically resolve cellular morphologies inside live brain tissue, both in slices and in live animals, which is rooted in STED microscopy being a laser beam *scanning microscopy* approach based on either confocal or 2-photon microscopy as the underlying modality, and thus comes with inherent good optical sectioning along the imaging z-axis. In contrast, the widefield techniques offer comparatively poor contrast along the z-axis in live tissue, because of out-of-focus fluorescence being collected that effectively blurs images. In practical terms, STED microscopy enables imaging in living brain tissue down to around 100 μm tissue depth (Urban et al., 2011), whereas the SMLM techniques are more suited for the surface of fixed brain slices and live imaging in dissociated cultures or smaller multicellular organisms. There are exceptions to this and SIM has recently been applied for *in vivo* imaging of synaptic structures, though in the diffraction limited non-saturated form that achieves maximally a 2-fold resolution enhancement, in this case around 190 nm (Turcotte et al., 2019). While this report of *in vivo* SIM is a great achievement that enables interesting studies because of the relatively high 9 Hz frame rate, it is still unable to geometrically resolve dendritic spine necks, axonal shafts, and other fine neural morphologies.

Another key advantage of STED is that it achieves super-resolution optically, without requiring digital image processing prior to visualization and analysis. It therefore comes closer to reporting the ground truth than techniques relying on computer-facilitated image reconstruction or deconvolution algorithms, which can be a genuine confounder for nanoscale structures (Sahl et al., 2016; Heintzmann and Huser, 2017; Karras et al., 2019).

For clarity, in this review we do not separately describe the reversible saturable optical fluorescence transitions (RESOLFT) technique that is very similar to STED, we only note here that it has also been applied for proof of principle live imaging in brain slices and *in vivo* in *C. elegans* worms (Testa et al., 2012; Dreier et al., 2019), and refer interested readers to a recent overview (Sahl and Hell, 2019).

2. Principles of STED microscopy

In fluorescence microscopy, *super-resolution* techniques refers to microscopy approaches that can optically resolve structures that fall

beyond the resolution limiting *diffraction barrier* formulated by Abbe (Abbe, 1882) and stated below (Eq. (1)). Diffraction is an inevitable physical phenomenon of waves, hereunder light, that causes them to bend as they interact with an object. Given that diffraction is inevitable, the best-case scenario for fluorescence microscopy performance is to be diffraction-limited. This infers the beam is then free from aberrations or any distortions of the beam wave front that lowers imaging resolution. The smallest point response a microscope can deliver is known as the *point-spread function* (PSF) and can be visualized and analyzed by imaging point sources, such as fluorescent beads that are substantially smaller than the PSF itself. Point sources will appear laterally as blurry spots with an approximate Gaussian intensity distribution, and PSF width can be determined from an intensity profile plot through the PSF image and extracting the width at the half-maximum height of the corresponding Gaussian fit. This is routinely referred to as the *full width at half maximum* (FWHM) (Cole et al., 2011), and is generally accepted as a proxy for optical resolution. In addition to Gaussian fitting, the FWHM of Lorentzian fits to point source PSFs are also commonly reported, as reviewed in (Lenz and Tønnesen, 2019). An alternative approach is to analyze the spatial frequencies that a STED image contains by means of Fourier transformation, and then determine the effective spatial cutoff frequency to represent the optical resolution limit (Banterle et al., 2013; Tortarolo et al., 2018). Resolution can additionally be assessed by imaging specially designed fluorescent nanorulers of well-defined length (Schmied et al., 2014; Lin et al., 2020).

Sample structures that are smaller than the PSF, and thus not geometrically resolved, do not simply disappear in images, but instead act as point-sources and appear blurred at the size of the PSF (Fig. 1A). Blurring also becomes evident across small distances between structures, where objects will appear to merge into a single structure if they are closer together than the size of the PSF. This can be didactically explained as drawing on top of a fine-lined sketch with a large-tipped marker pen, with the PSF corresponding to the pen tip.

In the case of all optical components being perfect, diffraction-limited optical resolution scales with the wavelength (λ) of the utilized light, and the numerical aperture of the microscope objective, *i.e.* the acceptance angle of the objective. The lateral resolution in the form of the PSF FWHM is then given by

$$r_{xy} \approx \frac{\lambda}{2NA} \quad (1)$$

where r_{xy} is the lateral resolution, λ is the excitation light wavelength, and *NA* the objective numerical aperture.

To understand how STED and other super-resolution microscopy modalities work, it is fundamental to keep in mind that 1) all involved laser beams are diffraction limited, also when the PSF is shaped into a specific form, *e.g.* a doughnut shape as in STED microscopy; 2) the resolution enhancement emerges as a product of the interaction between the diffraction limited PSFs of the incoming beams and the fluorophore population they interact with. That is, super-resolution is not only an optical phenomenon, but emerges from the interaction of diffraction-limited light with a given fluorophore population; hence the 2014 Nobel Prize to the inventors of super-resolution microscopy was in the category chemistry, not physics as one may have intuitively thought (Choquet, 2014). In conventional microscopy the excitation light PSF is linearly translated into a practically identical fluorescence emission PSF, at least as long as excitation is not saturated, which is practically never the case. The achievable spatial resolution is accordingly defined by the given excitation wavelength and optical components of the microscope, *i.e.* it is purely based on optics. On the contrary, in STED microscopy the emission PSF is not a simple linear translation of the excitation PSF, but is additionally molded by a second incoming laser beam. The achievable resolution of a STED setup is therefore not merely a constant property of the microscope hardware, but is tunable and varies with the observed fluorophore type and laser powers.

In the case of STED microscopy with resolution enhancement in the lateral plane, this is achieved by suppressing spontaneous fluorescence emission emerging from the periphery of the diffraction limited excitation PSF, so that the emission PSF effectively becomes smaller than the diffraction limit would otherwise allow (Harke et al., 2008). To achieve this, the STED beam PSF is engineered into a doughnut shape of a high intensity ring with a 0-intensity center and is superimposed on the Gaussian excitation beam PSF. The Gaussian excitation PSF brings fluorophores to the excited state, where they linger for a few nanoseconds, determined by the fluorophore fluorescence lifetime, before they spontaneously relax back to the ground state by emitting a photon. During

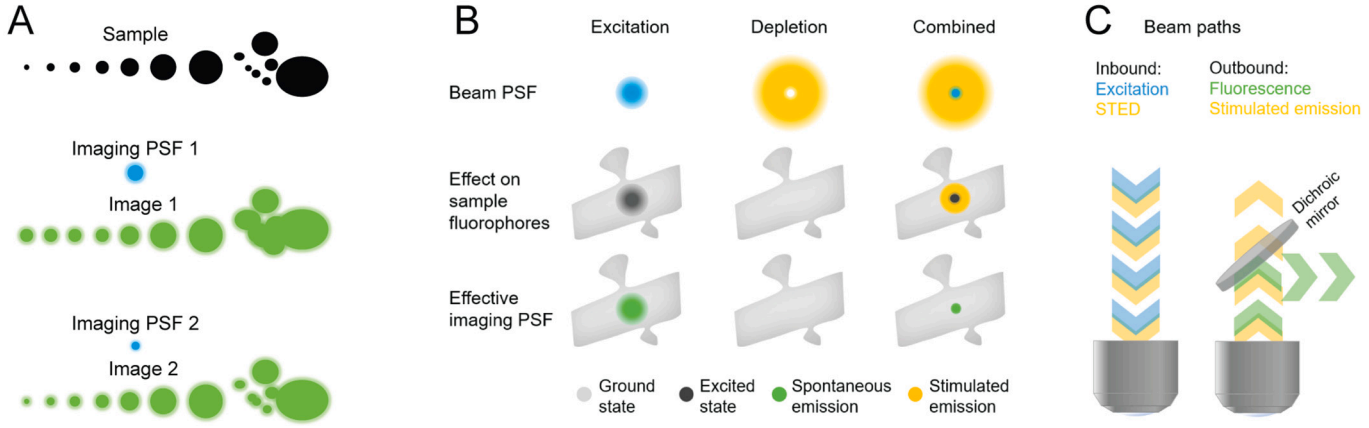

Fig. 1. Shaping PSFs to increase imaging resolution in STED. (**A**) In scanning fluorescence microscopy the sample is convolved by the effective imaging PSF, and structures that are smaller than the PSF itself will act as point-sources and appear at the size of the PSF. Accordingly, small structures appear larger than what they are, and objects closer together than the size of the PSF erroneously appear to merge. As imaging resolution is increased, more sub-diffraction structures and details become discernible. (**B**) In conventional scanning fluorescence microscopy, the excitation PSF brings the underlying fluorophore population linearly into the excited state and is translated 1:1 into an emission PSF. The doughnut shaped stimulated emission PSF has negligible effect on fluorophores in the ground state, but when superimposed on the excitation PSF it causes stimulated emission of fluorophores in the excited state. The STED beam intensity is high enough to saturate stimulated emission and efficiently deplete the excited state, so that only fluorophores in the doughnut zero-intensity center are allowed to emit spontaneous fluorescence. The area of spontaneous emission is increasingly spatially confined by higher STED beam powers to further enhance the effective imaging resolution. (**C**) The orange stimulated emission beam used for STED microscopy of green fluorophores is separated along with the blue spectrum excitation beam from the green spontaneous fluorescence by a simple dichroic mirror, allowing high contrast detection of the super-resolved spontaneous fluorescence signal. (For interpretation of the references to color in this figure legend, the reader is referred to the web version of this article.)

their nanosecond-long stay at the excited state, spontaneous emission can be prevented by forced, stimulated emission at a longer wavelength of less photonic energy than spontaneously emitted photons (Einstein, 1917), which is exactly the role of the STED beam PSF (Fig. 1B).

Stimulated emission can only occur within the normal spontaneous emission spectrum of a fluorophore, and usually the very edge towards longer wavelengths of the spectrum is used, *e.g.* in the orange range for green fluorophores. This lowers the probability of unwarranted direct fluorophore excitation by the STED beam, and leaves ample room for collecting the green spectrum light emerging from the doughnut center, where emission is not stimulated but occurs spontaneously as fluorescence. In essence, if a fluorophore in the excited state is hit by a photon of slightly longer wavelength than the photon that is otherwise emitted spontaneously, two photons identical to the (STED) photon hitting the fluorophore will be emitted. That is, two photons hit the fluorophore (one for excitation, one for stimulated emission) and two are emitted (identical to the incoming stimulated emission photon). The notable effect is that the photons emitted as spontaneous fluorescence and those emerging through stimulated emission have different wavelengths and can be easily separated by spectral filters into distinct beam paths. Thus, the spontaneously emitted fluorescence signal can be detected as in conventional confocal or 2-photon microscopy after discarding the stimulated emission signal by standard chromatic emission filters (Fig. 1C).

The optical resolution in STED microscopy scales with the square root of STED beam power, and Abbe's formula is extended to incorporate the STED effect as

$$r_{xy} \approx \frac{\lambda}{2NA\sqrt{(1 + (I/I_{sat}))}} \quad (2)$$

where I is the applied STED beam power, and I_{sat} is the STED power required to reduce the probability of spontaneous fluorescence emission by half (Harke et al., 2008). As can be understood, the STED beam intensity can be tuned for a specific sample to balance resolution, bleaching/toxicity, and contrast. Accordingly, when ensemble imaging densely labeled neurons, the higher the achieved resolution enhancement, the more photons are effectively discarded through stimulated emission and the weaker the collected fluorescence signal becomes. As electrical noise from the photodetector remains largely constant in the detected signal, the signal to noise ratio may consequently decrease. This is rarely an issue in live cell STED imaging utilizing highly sensitive photodiode detectors that usually have negligible dark counts (as observed in the figures below). Yet, it serves to convey the message that if super-resolution is not necessary, conventional confocal or 2-photon microscopy will often provide brighter images and potentially higher contrast, especially if imaging weakly fluorescent samples or samples with high background signal.

STED microscopy can be performed either with picosecond pulsed lasers or continuous wave (CW) lasers that emit at constant intensity. The combination of pulsed excitation and pulsed depletion is more technically elaborate, as the respective pulse trains have to be synchronized and aligned in space and time to achieve optimal STED. In contrast, STED microscopy using CW lasers has no such temporal synchronization requirement and is thus technically simpler (Willig et al., 2007). On the downside, the time-averaged depletion beam power in CW STED is around 4-fold higher than corresponding pulsed beam STED (Willig et al., 2007), making it less suitable for live imaging because of phototoxicity.

As STED microscopy relies on the use of two lasers for imaging a given fluorophore population, two-color imaging requires special consideration. If spectrally different fluorophores are used, *e.g.* green and red ones, it may be necessary to have separate excitation and STED beam pairs for these, which adds substantial technical complexity and requires twice the amount of photons compared to single channel acquisitions (Donnert et al., 2007). In fixed samples this is of little concern, though it may give rise to adverse effects on live neurons by unwarranted direct excitation of fluorophores by the STED beam or toxicity from tissue heating (Icha et al., 2017). It is also possible to use a common STED laser for two separate fluorophores excited by different laser sources (Pellett et al., 2011), to use photo-switching at a third wavelength to enable two fluorophores to be consecutively imaged by the same laser beam pair (Willig et al., 2011), or to separate fluorophores not spectrally, but instead based on fluorescence lifetime to facilitate two-color imaging with a single beam pair (Bückers et al., 2011). The simplest approach uses spectrally related fluorophores that can be excited by the same beam pair and do not rely on additional lasers compared to single-channel imaging, yet can be spectrally discerned. This approach comes with inherent spatial co-alignment and simultaneous acquisition of the two channels, factors that are critical for co-localization analyses of dynamic cellular structures (Tønnesen et al., 2011). The single beam-pair and spectral detection approach can be used to image green and yellow fluorophores alongside each other, and works for all fluorophore combinations we have tested, including among others: green and yellow fluorescent protein (GFP/YFP), GFP/Atto-514, YFP/Alexa Fluor 488, YFP/calcein, Alexa Fluor 514/Calcein. While the two detection channels spectrally overlap, all photons are effectively collected and contribute in the final image, with fluorophore discrimination unambiguously achieved already in the raw images, and further separation of the two overlapping channels into separate fluorophores through linear spectral unmixing (Tønnesen et al., 2011; Tønnesen and Nagerl, 2013).

3. The nanoscale morphologies of neural cells fall beyond the diffraction barrier

Synaptic structures in the form of dendritic spines, axonal shafts and boutons are among the key morphological features that are not resolved by conventional microscopy, and thus cannot be analyzed geometrically on live cells (Arellano et al., 2007; Mishchenko et al., 2010). The same limitation holds true for the fine processes of microglia and astrocytes that are known to shape synaptic signaling (Calì et al., 2019). Delineating the structure-function relationships of these specific cellular compartments is fundamental for understanding signal processing in the brain, and here the resolving power of STED microscopy comes to its right, as the obtainable 50 nm resolution covers the vast majority of neural cell morphological features. Smaller structures, for example scaffolding proteins and synaptic vesicles, remain more challenging to resolve in STED microscopy, and here electron microscopy (EM) and SMLM approaches may be superior.

EM has provided nanoscale resolution images of brain tissue for decades, and has been the almost exclusive source of such data until well into the 2000s (Harris and Weinberg, 2012). However, it is incompatible with live cell experiments and inescapably relies on tissue fixation, thereby preventing longitudinal experiments and parallel functional experiments, such as electrophysiological recordings. The emergence of structural artifacts resulting from fixation steps has long been a matter of concern when analyzing neural cell morphologies. It is generally accepted that cryo-fixation by rapid freezing of the sample better preserves the tissue ultrastructure, while the more commonly applied chemical fixation is associated with structural artifacts (van Harreveld and Crowell, 1964; Korogod et al., 2015; Tamada et al., 2020).

The roles of EM and fluorescence microscopy were long sharply divided; EM could provide nanoscale snapshots of morphology, while fluorescence microscopy offered live tissue experiments and allowed concurrent synergistic functional approaches, such as electrophysiology and pharmacology, though at mere microscale optical resolution. This gap is partially closing as the super-resolution modalities are now able to image at nanoscale resolution in live cells and tissue. The two approaches have been synergistically combined for correlative light and electron microscopy (CLEM) applied on the same sample, which has further been performed with SMLM to harness the best parts of both

modalities (Watanabe et al., 2011), though this is again only possible in fixed tissue.

Classic 2D-STED microscopy can provide around 50 nm lateral resolution in live tissue, though there is no resolution enhancement along the axial z-plane, with z-axis resolution typically around 500 nm for green fluorophores excited at 485 nm through high numerical aperture (1.2–1.4 NA) objectives (Cole et al., 2011). In 3D-STED, resolution is enhanced also along the axial plane, and typically reaches 150–250 nm (Wildanger et al., 2009; Lenz et al., 2014; Osseforth et al., 2014). This is still considerably lower than the lateral plane resolution around 50 nm, and lower than what can be achieved in EM, where the z-axis resolution is defined by the slice-cutting interval. In STED microscopy, the main analyses are therefore usually done in the lateral plane, while disregarding the axial plane, or simply assuming isotropic structures. The assumption of isotropy is justified for the analyses of dendrites, spines, axons and boutons that can be considered roughly cylindrical around their propagation axis, though for putatively more advanced analyses this assumption may be inadequate. Indeed, there is a need for better analysis methods to extract further, and more accurate, geometric structure parameters from STED images in an automated and unbiased way. In acknowledgement of this need, we recently contributed in the development of an ImageJ plugin called SpineJ to specifically analyze the geometry of dendritic spines in super-resolved images (Levet et al., 2020). Even so, there is therefore still ample room for technical

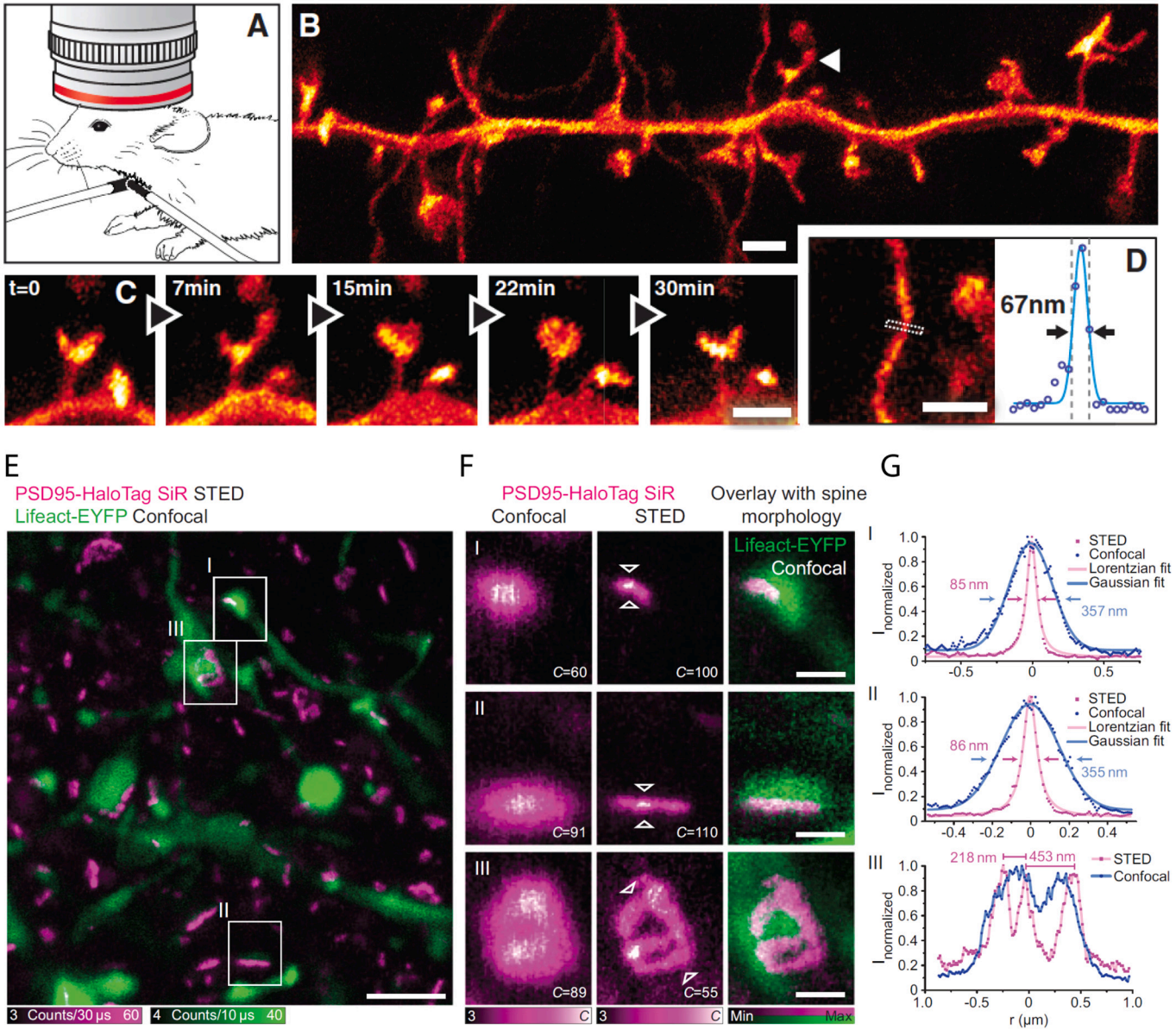

Fig. 2. STED microscopy of synaptic structures *in vivo*. (**A**) Schematic drawing of *in vivo* STED imaging setup. A high numerical aperture glycerol immersion objective is used to image neurons at the cortical surface through a glass cranial window. Tracheal tubes deliver anesthesia and are used for ventilation. (**B**) Dendritic segment of YFP labeled cortical neuron imaged *in vivo*. Scale bar is 1 µm. (**C**) Time-lapse image sequence illustrating spine head dynamic (Scale bar is 1 µm). (**D**) Zoomed-in view on super-resolved cellular structure (Scale bar is 1 µm). (**E**) *In vivo* STED microscopy of postsynaptic scaffold protein PSD-95 (PSD95-HaloTag SIR; magenta) and complementary confocal images of neuronal morphology (Lifeact-EYFP; green). Scale bar is 2 µm. (**F**) Zoom-ins on the squares in (E); STED microscopy reveals structural details of PSD-95 assemblies that are not visible in confocal images. Scale bars are 500 nm. (**G**) Comparisons of the FWHM of structures [between arrows depicted in (F)] imaged by both confocal and STED microscopy reveal the inadequacy of confocal for resolving PSD-95 assemblies. (A) to (D) from Berning et al., 2012, Science. Reprinted with permission from AAAS. (E) to (G) from Masch et al., 2018, PNAS, with permission (https://creativecommons.org/licenses/by/4.0/). (For interpretation of the references to color in this figure legend, the reader is referred to the web version of this article.)

improvements in optimizing STED imaging resolution, imaging depth, and image data extraction.

4. Technical developments of STED microscopy for live tissue imaging

Already the first experimental implementation of STED was impressively performed in live yeast cells (Klar et al., 2000), and in early 2008 the first STED images of live dissociated neurons emerged in the form of video-rate image sequences of synaptic vesicle movements (Westphal et al., 2008). Later the same year, the first proof-of-principle for STED microscopy in live brain tissue slices was reported (Nägerl et al., 2008), and in 2012 the first proof of principle for *in vivo* STED was provided as super-resolved time-lapse images of dendritic spines in the intact brain of a living mouse (Berning et al., 2012) (Fig. 2A–D). All these achievements came from the lab of Stefan Hell, the inventor of STED microscopy and Nobel Laureate, and while there are still relatively few labs committed to this type of experiments, a steadily increasing flow of technical developments and biological insights have continued to emerge, also from other groups. Among the more notable technical developments relevant for neuroscience research, two color STED microscopy in live cells (Pellett et al., 2011; Willig et al., 2011), and in live brain tissue (Tønnesen et al., 2011), was reported in 2011. Two-photon excitation STED imaging in live brain tissue was first reported in 2009 (Ding et al., 2009), and extended to 2-color imaging in 2013 (Bethge et al., 2013; Takasaki et al., 2013). While 2-photon excitation STED microscopy holds a great potential for imaging *in vivo* and inside tissue, it is still not widely applied, and still has not pushed the effective imaging depth beyond the around 100 μm achieved using single-photon excitation STED (Urban et al., 2011). In this respect, the implementation of microscope objectives with adjustable aberration correction-collars to enable deeper tissue imaging is noteworthy, because it allows rectification of spherical aberrations emerging from increasing tissue imaging depth, thus conserving the STED beam PSF and optical resolution (Urban et al., 2011). This type of aberration-correction objective has been used to image deeper *in vivo* (Wegner et al., 2017), in acute brain slices (Tønnesen et al., 2014), and in organotypic cultures (Urban et al., 2011).

The implementation of 3D-STED was, to some extent, realized already by the first reported STED experiments (Klar et al., 2000), though it has since been further developed (Wildanger et al., 2009; Lenz et al., 2014), extended to the 2-color regime (Osseforth et al., 2014), and more recently applied to living brain slices (Tønnesen et al., 2018), and *in vivo* (Velasco et al., 2021).

As already mentioned, *in vivo* STED microscopy was first implemented in 2012, and it has since been further developed to observe deep hippocampal tissue through implantable lenses in anaesthetized mice (Pfeiffer et al., 2018). Two-color STED is still to be reported in *in vivo* settings, though *in vivo* STED images of PSD-95 proteins superimposed on confocal images of spines have been reported, testifying to the applicability and versatility of STED to be applied along classical microscopy modalities (Masch et al., 2018) (Fig. 2E–G).

To recapitulate, 3D-STED microscopy can today be readily performed in two colors in live, cultured or acute, brain slices (Tønnesen et al., 2014, 2018), and in principle this technology can be directly transferred to *in vivo* settings, where single-color 2D and 3D-STED is already being utilized based on single or 2-photon excitation (Wegner et al., 2017, 2018; Pfeiffer et al., 2018; Steffens et al., 2020; Velasco et al., 2021).

5. Fluorophores and labeling strategies

The considerations associated with choice of fluorophores and labeling strategies for live cell STED microscopy are largely the same as for conventional live cell fluorescence microscopy, though with special consideration to the dual wavelength approach underlying STED, and the comparably higher involved laser powers.

Fluorescent labeling for STED microscopy of live cells can be done manually by patch-loading cells with fluorophores, such as Alexa or Atto dyes (Ding et al., 2009; Tønnesen et al., 2011; Chéreau et al., 2017) or filling them through bolus loading with acetoxymethyl (AM)-ester coupled fluorophores injected locally into tissue (Tønnesen et al., 2011). It is, however, often more convenient to utilize genetically encoded fluorophores when possible, to avoid perturbations of cells and tissue. This can be achieved through a viral-vector approach in cultured brain slices (Tønnesen et al., 2011; Urban et al., 2011; Chéreau et al., 2017) or *in vivo* (Wegner et al., 2017), plasmid transfection in cultured cells (Pellett et al., 2011; Willig et al., 2011), or any of the many available transgenic animals available, for example the popular Thy1-YFP mice that expresses YFP in subsets of excitatory neurons (Feng et al., 2000). More sophisticated utilization of transgene animals has been adopted to image specific synaptic structures, including postsynaptic PSD-95 scaffold proteins in live mice (Wegner et al., 2018).

An approach that bridges genetic and acute labeling is the genetic expression of polypeptide *tagged* proteins in combinations with organic fluorophores that bind to the tag. This is a 2-component approach that confers high labeling specificity. Commonly used are the SNAP sequence, which covalently conjugates with benzyl guanine (Keppler et al., 2003), and the Halo sequence, conjugating with chloro alkane (Los et al., 2008). A reported advantage of the tagging approach is the brightness and stability of the utilized organic dyes (Fernández-Suárez and Ting, 2008), with the Halo system appearing superior for STED microscopy in terms of brightness (Erdmann et al., 2019). SNAP, Halo, and CLIP tag labeling has been used for 2-color STED imaging in live cells (Pellett et al., 2011; Bottanelli et al., 2016), and more recently STED was applied *in vivo* to image Halo-tag fusion protein PSD-95 and map the complex spatial organization of protein clusters in the visual cortex surface (Masch et al., 2018).

Freely diffusible cytosolic fluorophores are convenient for imaging cellular morphologies in STED, because putative bleached fluorophores are to some extent replenished by diffusion of unbleached fluorophores from neighboring parts of the cytosol. This fluorophore diffusion further allows fluorescence recovery after photobleaching (FRAP) experiments to reveal diffusional compartmentalization in the imaged morphological structures (Takasaki and Sabatini, 2014; Tønnesen et al., 2014).

In terms of popularity and availability, fluorophores in the green spectrum are the most widespread across fluorescence microscopy, with most transgenic mice and viral vectors relying on GFP as the reporter. Though besides general availability, the spectral properties of fluorophores come with additional implications. One limiting factor has been the lack of appropriate pulsed lasers emitting in the orange spectrum required for stimulated emission of green/yellow fluorophores. The absence of such lasers necessitated complex and expensive STED setups relying on tunable femtosecond pulse lasers coupled with optical parametric oscillators (OPOs) to shift the wavelength from infrared to orange (Willig et al., 2006; Nägerl et al., 2008), which involves several tedious work routines. With the recent commercial availability of orange emitting picosecond lasers, these OPO based setups will likely soon be a memorable curiosity of the past.

As can be understood from Eq. (1) above, in conventional microscopy resolution scales directly with the utilized excitation wavelength, and the relatively short wavelengths used for imaging in the green spectrum already offer a notably better resolution than when imaging red fluorophores. On the other hand, red fluorophores are attractive because light in the red spectrum travels better in brain tissue to facilitate deeper imaging. This also holds true for STED microscopy, where red-shifted fluorophores facilitate deeper imaging *in vivo*, and resolution is anyways not limited by the excitation wavelength (Wegner et al., 2017). Green and yellow fluorophores can indeed also be STED imaged using infrared excitation light in the 2-photon excitation regime, which allows deeper imaging but comes at the price of increased cost for a femtosecond laser source, and a lower default diffraction limited

resolution compared to single-photon excitation confocal imaging (Ding et al., 2009; Bethge et al., 2013; Takasaki et al., 2013). A recent study reports improvements to reach 76 μm depth for *in vivo* STED microscopy with 3D resolution enhancement based on combined 2-photon excitation, adaptive optics, far-red emitting organic dyes, and a long-working distance water-immersion objective lens (Velasco et al., 2021). It is noteworthy that in 2-photon excitation-based STED microscopy, depletion wavelengths remain the same as for single-photon excitation STED, meaning the STED beam PSF will not be different between the two configurations and degrade similarly with increasing tissue depth. As a consequence, the expected resolution difference at depth between single- and 2-photon excitation STED microscopy may be less evident than one may initially expect, though a head-to-head comparison has not been performed.

6. Neurobiological insights from STED microscopy

The unique ability of STED microscopy to provide nanoscale resolution images of neural structures in live brain tissue has provided neurophysiological data that would not readily be deliverable by alternative techniques. This technology has allowed examination of the central nervous system at an unprecedented scale, improving our understanding of the cellular and molecular mechanisms that govern brain function. Here we highlight the main findings, with a focus on studies in live tissue.

The morphological dynamics of dendritic spines, and their role in regulating synaptic function, have long been an enigmatic subject in neuroscience. Fifková and Anderson noted differences in the structure of dendritic spines when comparing populations submitted to tetanic stimulation and controls (Fifková and Anderson, 1981). However, since this study relied on EM and fixed tissue experiments, they could not prove that the observed differences reflected spine structural dynamics rather than changes in spine morphological sub-populations. Indeed, around the same time, in 1982, Francis Crick asked "Do dendritic spines twitch rapidly during normal neural activity? If so, what are the rules governing the change of shape of the spine and, in particular, the neck of the spine?" (Crick, 1982), a question that stood unanswered for several more decades. Two-photon microscopy provided evidence for spine head enlargement in response to stimulation-induced synaptic long-term potentiation (LTP) (Matsuzaki et al., 2004), as well as for concurrent spine neck shortening (Tanaka et al., 2008). However, the key parameter from a biophysical perspective is spine neck *width*, which is predictably the primary determinant of biochemical and electrical compartmentalization of the residing synapse. Due to its nanoscale morphology, neck width could not be optically resolved by diffraction-limited methods, and putative spine neck width plasticity remained elusive for years, thus preventing direct application of cable theory in predicting the functional effects of putative spine neck dynamics (Wilson, 1984). In 2014, STED microscopy combined with 2-photon glutamate uncaging and FRAP experiments revealed that indeed during LTP the spine head grows, while the neck correspondingly shortens and widens (Tønnesen et al., 2014) (Fig. 3A–B). Biophysical modeling suggests that this results in a roughly 50% decrease in the electrical neck resistance to passing synaptic currents, while in terms of biochemical *sojourn* time the combined head and neck changes result in a zero-sum scenario (Tønnesen and Nägerl, 2016). Interestingly, this provides evidence for separate functional roles of respective spine head and neck morphology, whereby neck dynamics affect both electrical and biochemical compartmentalization, while head dynamics exclusively affect biochemical compartmentalization. The correlation between spine morphology and biochemical diffusional properties has further been confirmed by 2-photon excitation STED microscopy in acute brain slices (Takasaki and Sabatini, 2014).

The effect of dendrite and dendritic spine morphology on inhibitory synaptic signaling has been modeled using STED images of live neurons in brain slices. STED images allowed more accurate predictions on the intra-dendritic spreading of chloride transients, and contributed in identifying a key role for spine density and morphology in short-term ionic plasticity of inhibitory GABA receptor mediated signaling (Mohapatra et al., 2016).

Another key finding from live tissue STED microscopy is that when imaged at diffraction-limited optical resolution, short-necked dendritic spines will commonly appear erroneously stubby, *i.e.* without a discernible neck. This was observed both in slices (Tønnesen et al., 2014), and during chronic *in vivo* STED imaging of dendritic spines in hippocampus, where closely neighboring spines would erroneously appear as one when imaged by 2-photon microscopy (Pfeiffer et al., 2018). Similar observations have been reported in fixed tissue (Attardo et al., 2015). The mentioned *in vivo* STED study by Pfeiffer and colleagues further found that some 40% of hippocampal dendritic spines turned over in 4 days. This value suggests a middle-ground between those reported in two highly discrepant 2-photon microscopy studies, one reporting that 96% of spines remained stable over 16 days (Gu et al., 2014), while the other suggesting nearly 100% turnover within 2–3 weeks (Attardo et al., 2015). The remarkable discrepancy between these three studies warrants further research, and could indicate that the given experimental settings directly impact spine turnover rates.

The cytoskeleton plays a critical role in shaping cell morphology and organizing intracellular compartments. However, its fine structure has been elusive due to its diffraction-limited scale. Using STORM in fixed cells, axons were shown to contain highly regular periodic actin- and spectrin-containing rings at 180 to 190 nm intervals (Xu et al., 2013). Such rings have been recently demonstrated with STED microscopy, also in dendritic spine necks in neurons from both acute and organotypic slices, and with a similar interval around 180 to 190 nm (Bär et al., 2016). This extends other findings using STED microscopy in live dissociated neurons that found similar periodic rings in dendrites and axons (D'Este et al., 2015), unraveling unique cytoskeletal features that influence the distribution of receptors and channels in the cell membrane.

Neef and colleagues took advantage of STED microscopy to not only image inner hair cells, but also perform super-resolution calcium imaging to identify calcium signaling domains associated with presynaptic active zones (Neef et al., 2018). Calcium imaging at increased spatial resolution holds special interest for physiologists, where calcium transients are expected to be compartmentalized. While it may be spatially resolved, the diffusion of ionic calcium is still too fast to be *temporally* resolved.

Axons convey action potentials to pre-synaptic boutons where they cause transmitter release as part of synaptic signaling. The axon has classically been considered structurally static, with membrane ion channels as the primary regulators of conduction velocity (Sasaki et al., 2011). However, STED microscopy in live brain slices was able to geometrically resolve axons during high frequency action potential firing, and demonstrate that this activity was associated with axon widening and a corresponding increase in action potential conduction velocity (Chéreau et al., 2017). The resolving power of STED microscopy in these experiments was key for performing the advanced comparative analysis of structural axon dynamics and electrophysiological recordings of action potential firing.

In addition to neurons, glial cells have extremely complex morphologies and are not geometrically resolved by diffraction-limited microscopy modalities. This has hindered the structure-function delineation of the tripartite synapse consisting of neuronal pre- and post-synaptic compartments, in addition to an astrocytic partner (Araque et al., 1999). STED microscopy in organotypic brain slices was recently applied alongside calcium imaging to show that astrocytic calcium signals occur in nodes that are frequently associated with dendritic spines (Arizono et al., 2020). In a separate recent study, STED was applied to demonstrate withdrawal of perisynaptic astrocytic processes following LTP induction in live organotypic slices, effectively facilitating glutamate spillover (Henneberger et al., 2020). While also microglia (Bethge

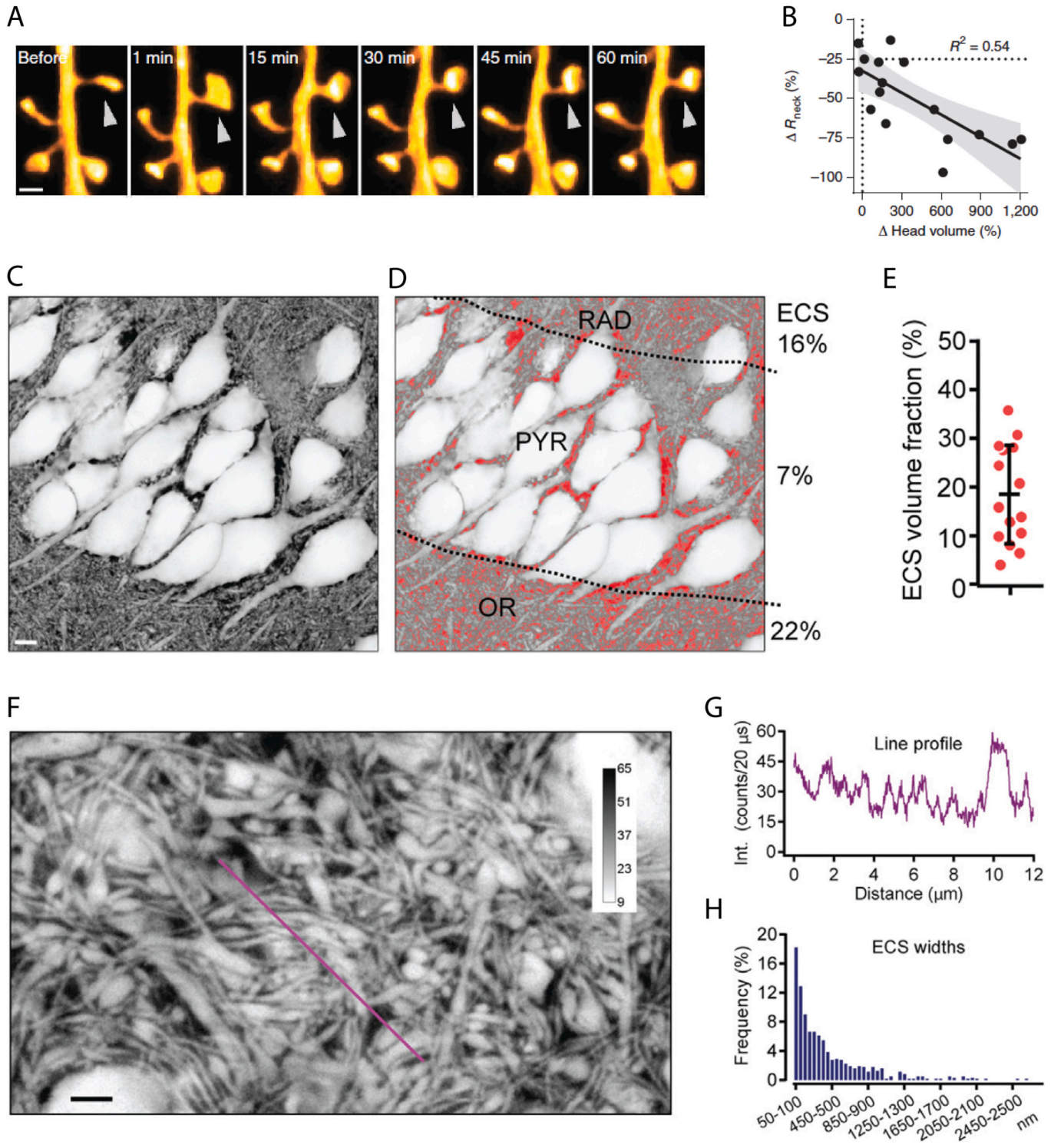

Fig. 3. New insights from STED microscopy in live tissue. (**A**) Time-lapse STED image sequence of dendritic spine (identified by arrow) undergoing LTP after 2-photon glutamate uncaging stimulation. LTP is associated with spine head enlargement and spine neck shortening and widening. Scale bar is 500 nm. (**B**) The calculated changes in electrical spine neck resistance (R_{neck}) and head volume expansion correlate strongly, suggesting coordination between these changes. (**C**) SUSHI image of the CA1 area reveal unlabeled cells (bright) and the surrounding ECS (dark) perfusion labeled by a fluorophore that distributes homogenously in the interstitial fluid. Scale bar is 5 µm. (**D**) The SUSHI approach allows straightforward nanoscale analysis of the ECS (red) volume fraction, and shows this varies across the CA1 layers *oriens*, *pyramidale* and *radiatum*. (**E**) ECS volume fractions measured across various areas in hippocampal slices reveal large variation with an average value close to 20%. (**F**) SUSHI image of the neuropil (bright) and ECS (dark) in live brain tissue, revealing the intricate, interwoven neural structures. Scale bar is 2 µm. (**G**) Line-intensity profile of the image under the line depicted in (F). The peaks correspond to ECS channels, while troughs represent neural structures. (**H**) ECS channel width analysis across hippocampal slices reveals a continuum spanning from a few microns down to 50 nm, corresponding to the resolution limit of the utilized STED microscope. (A) and (B) from Tønnesen et al., 2014, Nat Neurosci. (C) to (H) from Tønnesen et al., 2018, Cell, with permission from Elsevier. (For interpretation of the references to color in this figure legend, the reader is referred to the web version of this article.)

et al., 2013) and oligodendrocytes (Steshenko et al., 2016) have been successfully observed in a STED microscope, these studies have focused more on the technique itself rather than on gaining a functional insight into these cell types.

Beyond imaging the intricate morphological structure and dynamics of neural cells, STED microscopy has been used to reveal the nanoscale structure and dynamics of the brain extracellular space (ECS) in live brain tissue, by combining 3D-STED imaging with perfusion labeling of the interstitial fluid (Tønnesen et al., 2018). Perfusion labeling with hydrophilic fluorophores that do not pass the cell membrane visualizes the interstitial fluid, which in structure corresponds to the ECS. The label can be applied acutely to unlabeled tissue by simple perfusion, and intensity easily adjusted on the fly by adding fluorophores or diluting these. As the concentration of fluorophore is constant in the ECS during perfusion labeling, intensity differences, at any scale, reflect ECS volume differences and can be analyzed quantitatively.

This particular approach, termed super-resolution shadow imaging (SUSHI), has provided the first structural images of ECS in live tissue, and identified previously unknown glutamate-induced microscale dynamics. SUSHI images inherently reveal the morphology of all unlabeled cells in the field of view as analyzable shadows, thereby enabling investigation of neural cells with respect to neighboring cells, the surrounding neuropil, and the ECS, all in a single frame acquisition (Fig. 3C–D). The diffusible extracellular label provides practical immunity to photobleaching and -toxicity, as bleached fluorophores and toxic species escape the field of view and are continuously replenished by intact fluorophores. This allows extensive 3D-STED time-lapse imaging of relatively large fields of view (*e.g.* 100 frames of 100 μm by 100 μm). By directly visualizing the ECS structure, this can be analyzed with respect to structural complexity and volume fraction (Fig. 3E–H), and the provided data are in good agreement with existing EM data from cryo-fixed tissue and data from volume-averaging live tissue-compatible techniques, as we have recently reviewed (Soria et al., 2020a).

7. Perspectives

STED microscopy is still unique among the super-resolution modalities in being particularly well suited for imaging in live brain tissue, either in slices or *in vivo*. By pushing the boundaries of the observable in live tissue, this technology has facilitated key insights, particularly into the dynamic geometry of synaptic structures. Despite these remarkable advances on the nanoscale physiology of neurons, research on glial cell physiology and the field of neurological disorders have so far received limited attention through live tissue STED imaging approaches, and there is a corresponding potential for scientific discoveries in this area.

Of particular interest in a pathological context is the application of STED imaging to diseases associated with dysmorphic dendritic spines, where it may be combined with optical or electrophysiological functional techniques to delineate whether altered spine structure represents a cause or effect of pathology, and the significance of altered spine structure in a disease context. Recent developments in combining STED and optogenetics are interesting here (Stahlberg et al., 2019), as are developments in tracking single-walled carbon-nanotubes moving through the ECS in live brain tissue (Godin et al., 2017). Directly related to this, the ability of STED to visualize the brain ECS in live tissue will be interesting for studying metabolite clearance *via* the glymphatic system in dense tissue, were knowledge is currently lacking (Iliff et al., 2012; Xie et al., 2013). Similarly, neurodegeneration is associated with substantial remodeling of the ECS (Soria et al., 2020b), though the consequences of these nanoscale changes for progressive pathology remain unknown. This can now more readily be explored by combining STED microscopy with existing and emerging complementary techniques, as well as new biophysical models harnessing the additional information by such approaches.

Furthermore, non-neuronal cellular morphologies are often affected in pathology, including myelinating oligodendrocyte processes and dynamically scanning microglia in different functional states, and these are now prime candidates for STED imaging (Bernier et al., 2019).

Live tissue STED microscopy is currently not widely adopted across labs, and STED microscopy is still primarily used in fixed tissue experiments. We hope this will change, as STED microscopy holds great potential for breakthrough discoveries when applied in live tissue experiments. Recent developments in laser technology have made it cheaper to implement and use, and still more oven-ready options are being offered commercially. This is all but certain to increase the number of labs embracing STED microscopy in general, and thereby its application in live tissue. Another important development is the establishment of new labs headed by people with adequate training in live tissue STED microscopy and its application in a neuroscientific context, where the emergence of this second generation of users is a fundamental step towards its broader use.

Acknowledgements

The authors acknowledge funding for their general work from the Spanish Ministry of Science and Innovation (SAF-2017-83776-R, RYC-2014-15994 and IJCI-2017-32114), the Basque Government (PIBA19-0065 and PIBA-2020-1-0061), and the University of the Basque Country (GIU18/094 and INF19-29).

References

Abbe, Ernst, 1882. The relation of aperture and power in the microscope. J. R. Microsc. Soc. 2, 300–309. https://doi.org/10.1111/j.1365-2818.1882.tb00190.x.

Araque, A., Parpura, V., Sanzgiri, R.P., Haydon, P.G., 1999. Tripartite synapses: glia, the unacknowledged partner. Trends Neurosci. 22, 208–215. https://doi.org/10.1016/S0166-2236(98)01349-6.

Arellano, J.I., Benavides-Piccione, R., DeFelipe, J., Yuste, R., 2007. Ultrastructure of dendritic spines: correlation between synaptic and spine morphologies. Front. Neurosci. 1 https://doi.org/10.3389/neuro.01.1.1.010.2007.

Arizono, M., Inavalli, V.V.G.K., Panatier, A., Pfeiffer, T., Angibaud, J., Levet, F., et al., 2020. Structural basis of astrocytic Ca 2+ signals at tripartite synapses. Nat. Commun. 11, 1906. https://doi.org/10.1038/s41467-020-15648-4.

Attardo, A., Fitzgerald, J.E., Schnitzer, M.J., 2015. Impermanence of dendritic spines in live adult CA1 hippocampus. Nature 523, 592–596. https://doi.org/10.1038/nature14467.

Banterle, N., Bui, K.H., Lemke, E.A., Beck, M., 2013. Fourier ring correlation as a resolution criterion for super-resolution microscopy. J. Struct. Biol. 183, 363–367. https://doi.org/10.1016/j.jsb.2013.05.004.

Bär, J., Kobler, O., van Bommel, B., Mikhaylova, M., 2016. Periodic F-actin structures shape the neck of dendritic spines. Sci. Rep. 6, 37136. https://doi.org/10.1038/srep37136.

Bernier, L.-P., Bohlen, C.J., York, E.M., Choi, H.B., Kamyabi, A., Dissing-Olesen, L., et al., 2019. Nanoscale surveillance of the brain by microglia via cAMP-regulated Filopodia. Cell Rep. 27, 2895–2908.e4.

Berning, S., Willig, K.I., Steffens, H., Dibaj, P., Hell, S.W., 2012. Nanoscopy in a living mouse brain. Science 335, 551. https://doi.org/10.1126/science.1215369.

Bethge, P., Chéreau, R., Avignone, E., Marsicano, G., Nägerl, U.V., 2013. Two-photon excitation STED microscopy in two colors in acute brain slices. Biophys. J. 104, 778–785. https://doi.org/10.1016/j.bpj.2012.12.054.

Betzig, E., Patterson, G.H., Sougrat, R., Lindwasser, O.W., Olenych, S., Bonifacino, J.S., et al., 2006. Imaging intracellular fluorescent proteins at nanometer resolution. Science 313, 1642–1645. https://doi.org/10.1126/science.1127344.

Bottanelli, F., Kromann, E.B., Allgeyer, E.S., Erdmann, R.S., Baguley, S.W., Sirinakis, G., et al., 2016. Two-colour live-cell nanoscale imaging of intracellular targets. Nat. Commun. 7, 10778. https://doi.org/10.1038/ncomms10778.

Bückers, J., Wildanger, D., Vicidomini, G., Kastrup, L., Hell, S.W., 2011. Simultaneous multi-lifetime multi-color STED imaging for colocalization analyses. Opt. Express 19, 3130–3143.

Calì, C., Agus, M., Kare, K., Boges, D.J., Lehväslaiho, H., Hadwiger, M., et al., 2019. 3D cellular reconstruction of cortical glia and parenchymal morphometric analysis from Serial Block-Face Electron Microscopy of juvenile rat. Prog. Neurobiol. 183, 101696. https://doi.org/10.1016/j.pneurobio.2019.101696.

Centonze, V., Pawley, J., 1995. Tutorial on practical confocal microscopy and use of the confocal test specimen. In: Pawley, J.B. (Ed.), Handbook of Biological Confocal Microscopy. Springer US, Boston, MA, pp. 549–569. https://doi.org/10.1007/978-1-4757-5348-6_36.

Chen, B.-C., Legant, W.R., Wang, K., Shao, L., Milkie, D.E., Davidson, M.W., et al., 2014. Lattice light-sheet microscopy: imaging molecules to embryos at high spatiotemporal resolution. Science 346, 1257998. https://doi.org/10.1126/science.1257998.

Chen, F., Tillberg, P.W., Boyden, E.S., 2015. Expansion microscopy. Science 347, 543–548. https://doi.org/10.1126/science.1260088.

Chéreau, R., Saraceno, G.E., Angibaud, J., Cattaert, D., Nägerl, U.V., 2017. Superresolution imaging reveals activity-dependent plasticity of axon morphology

linked to changes in action potential conduction velocity. Proc. Natl. Acad. Sci. U. S. A. 114, 1401–1406. https://doi.org/10.1073/pnas.1607541114.
Choquet, D., 2014. The 2014 Nobel prize in chemistry: a large-scale prize for achievements on the nanoscale. Neuron 84, 1116–1119. https://doi.org/10.1016/j.neuron.2014.12.002.
Cole, R.W., Jinadasa, T., Brown, C.M., 2011. Measuring and interpreting point spread functions to determine confocal microscope resolution and ensure quality control. Nat. Protoc. 6, 1929–1941. https://doi.org/10.1038/nprot.2011.407.
Crick, F., 1982. Do dendritic spines twitch? Trends Neurosci. 5, 44–46. https://doi.org/10.1016/0166-2236(82)90020-0.
Dempsey, G.T., Vaughan, J.C., Chen, K.H., Bates, M., Zhuang, X., 2011. Evaluation of fluorophores for optimal performance in localization-based super-resolution imaging. Nat. Methods 8, 1027–1036. https://doi.org/10.1038/nmeth.1768.
D'Este, E., Kamin, D., Göttfert, F., El-Hady, A., Hell, S.W., 2015. STED nanoscopy reveals the ubiquity of subcortical cytoskeleton periodicity in living neurons. Cell Rep. 10, 1246–1251. https://doi.org/10.1016/j.celrep.2015.02.007.
Ding, J.B., Takasaki, K.T., Sabatini, B.L., 2009. Supraresolution imaging in brain slices using stimulated-emission depletion two-photon laser scanning microscopy. Neuron 63, 429–437. https://doi.org/10.1016/j.neuron.2009.07.011.
Donnert, G., Keller, J., Wurm, C.A., Rizzoli, S.O., Westphal, V., Schönle, A., et al., 2007. Two-color far-field fluorescence nanoscopy. Biophys. J. 92, L67–L69. https://doi.org/10.1529/biophysj.107.104497.
Dreier, J., Castello, M., Coceano, G., Cáceres, R., Plastino, J., Vicidomini, G., et al., 2019. Smart scanning for low-illumination and fast RESOLFT nanoscopy in vivo. Nat. Commun. 10, 556. https://doi.org/10.1038/s41467-019-08442-4.
Einstein, A., 1917. Zur Quantentheorie der Strahlung. Phys. Z. 18. Available at: http://adsabs.harvard.edu/abs/1917PhyZ...18..121E.
Erdmann, R.S., Baguley, S.W., Richens, J.H., Wissner, R.F., Xi, Z., Allgeyer, E.S., et al., 2019. Labeling strategies matter for super-resolution microscopy: a comparison between HaloTags and SNAP-tags. Cell Chem. Biol. 26, 584–592.e6. https://doi.org/10.1016/j.chembiol.2019.01.003.
Feng, G., Mellor, R.H., Bernstein, M., Keller-Peck, C., Nguyen, Q.T., Wallace, M., et al., 2000. Imaging neuronal subsets in transgenic mice expressing multiple spectral variants of GFP. Neuron 28, 41–51. https://doi.org/10.1016/S0896-6273(00)00084-2.
Fernández-Suárez, M., Ting, A.Y., 2008. Fluorescent probes for super-resolution imaging in living cells. Nat. Rev. Mol. Cell Biol. 9, 929–943. https://doi.org/10.1038/nrm2531.
Fifková, E., Anderson, C.L., 1981. Stimulation-induced changes in dimensions of stalks of dendritic spines in the dentate molecular layer. Exp. Neurol. 74, 621–627.
Godin, A.G., Varela, J.A., Gao, Z., Danné, N., Dupuis, J.P., Lounis, B., et al., 2017. Single-nanotube tracking reveals the nanoscale organization of the extracellular space in the live brain. Nat. Nanotechnol. 12, 238–243. https://doi.org/10.1038/nnano.2016.248.
Gu, L., Kleiber, S., Schmid, L., Nebeling, F., Chamoun, M., Steffen, J., et al., 2014. Long-term in vivo imaging of dendritic spines in the hippocampus reveals structural plasticity. J. Neurosci. 34, 13948–13953. https://doi.org/10.1523/JNEUROSCI.1464-14.2014.
Gustafsson, M.G.L., 2000. Surpassing the lateral resolution limit by a factor of two using structured illumination microscopy. J. Microsc. 198, 82–87. https://doi.org/10.1046/j.1365-2818.2000.00710.x.
Gustafsson, M.G.L., 2005. Nonlinear structured-illumination microscopy: wide-field fluorescence imaging with theoretically unlimited resolution. Proc. Natl. Acad. Sci. U. S. A. 102, 13081–13086. https://doi.org/10.1073/pnas.0406877102.
Gwosch, K.C., Pape, J.K., Balzarotti, F., Hoess, P., Ellenberg, J., Ries, J., et al., 2020. MINFLUX nanoscopy delivers 3D multicolor nanometer resolution in cells. Nat. Methods 17, 217–224. https://doi.org/10.1038/s41592-019-0688-0.
Harke, B., Keller, J., Ullal, C.K., Westphal, V., Schönle, A., Hell, S.W., 2008. Resolution scaling in STED microscopy. Opt. Express 16, 4154–4162.
van Harreveld, A., Crowell, J., 1964. Electron microscopy after rapid freezing on a metal surface and substitution fixation. Anat. Rec. 149, 381–385. https://doi.org/10.1002/ar.1091490307.
Harris, K.M., Weinberg, R.J., 2012. Ultrastructure of synapses in the mammalian brain. Cold Spring Harb. Perspect. Biol. 4, a005587. https://doi.org/10.1101/cshperspect.a005587.
Heintzmann, R., Huser, T., 2017. Super-resolution structured illumination microscopy. Chem. Rev. 117, 13890–13908. https://doi.org/10.1021/acs.chemrev.7b00218.
Hell, S.W., Wichmann, J., 1994. Breaking the diffraction resolution limit by stimulated emission: stimulated-emission-depletion fluorescence microscopy. Opt. Lett. 19, 780–782. https://doi.org/10.1364/OL.19.000780.
Henneberger, C., Bard, L., Panatier, A., Reynolds, J.P., Kopach, O., Medvedev, N.I., et al., 2020. LTP induction boosts glutamate spillover by driving withdrawal of perisynaptic Astroglia. Neuron 108, 919–936.e11. https://doi.org/10.1016/j.neuron.2020.08.030.
Hess, S.T., Girirajan, T.P.K., Mason, M.D., 2006. Ultra-high resolution imaging by fluorescence photoactivation localization microscopy. Biophys. J. 91, 4258–4272. https://doi.org/10.1529/biophysj.106.091116.
Huisken, J., Swoger, J., Bene, F.D., Wittbrodt, J., Stelzer, E.H.K., 2004. Optical sectioning deep inside live embryos by selective plane illumination microscopy. Science 305, 1007–1009. https://doi.org/10.1126/science.1100035.
Icha, J., Weber, M., Waters, J.C., Norden, C., 2017. Phototoxicity in live fluorescence microscopy, and how to avoid it. BioEssays 39, 1700003. https://doi.org/10.1002/bies.201700003.
Iliff, J.J., Wang, M., Liao, Y., Plogg, B.A., Peng, W., Gundersen, G.A., et al., 2012. A paravascular pathway facilitates CSF flow through the brain parenchyma and the clearance of interstitial solutes, including amyloid β. Sci. Transl. Med. 4, 147ra111 https://doi.org/10.1126/scitranslmed.3003748.
Jahr, W., Velicky, P., Danzl, J.G., 2020. Strategies to maximize performance in STimulated Emission Depletion (STED) nanoscopy of biological specimens. Methods San Diego Calif. 174, 27–41. https://doi.org/10.1016/j.ymeth.2019.07.019.
Karras, C., Smedh, M., Förster, R., Deschout, H., Fernandez-Rodriguez, J., Heintzmann, R., 2019. Successful optimization of reconstruction parameters in structured illumination microscopy – a practical guide. Opt. Commun. 436, 69–75. https://doi.org/10.1016/j.optcom.2018.12.005.
Keppler, A., Gendreizig, S., Gronemeyer, T., Pick, H., Vogel, H., Johnsson, K., 2003. A general method for the covalent labeling of fusion proteins with small molecules in vivo. Nat. Biotechnol. 21, 86–89. https://doi.org/10.1038/nbt765.
Khater, I.M., Nabi, I.R., Hamarneh, G., 2020. A review of super-resolution single-molecule localization microscopy cluster analysis and quantification methods. Patterns 1, 100038. https://doi.org/10.1016/j.patter.2020.100038.
Kim, J., Wojcik, M., Wang, Y., Moon, S., Zin, E.A., Marnani, N., et al., 2019. Oblique-plane single-molecule localization microscopy for tissues and small intact animals. Nat. Methods 16, 853–857. https://doi.org/10.1038/s41592-019-0510-z.
Klar, T.A., Jakobs, S., Dyba, M., Egner, A., Hell, S.W., 2000. Fluorescence microscopy with diffraction resolution barrier broken by stimulated emission. Proc. Natl. Acad. Sci. 97, 8206–8210. https://doi.org/10.1073/pnas.97.15.8206.
Kner, P., Chhun, B.B., Griffis, E.R., Winoto, L., Gustafsson, M.G.L., 2009. Super-resolution video microscopy of live cells by structured illumination. Nat. Methods 6, 339–342. https://doi.org/10.1038/nmeth.1324.
Korogod, N., Petersen, C.C.H., Knott, G.W., 2015. Ultrastructural analysis of adult mouse neocortex comparing aldehyde perfusion with cryo fixation. eLife 4. https://doi.org/10.7554/eLife.05793.
Lenz, M.O., Tønnesen, J., 2019. Considerations for imaging and analyzing neural structures by STED microscopy. Methods Mol. Biol. Clifton NJ 1941, 29–46. https://doi.org/10.1007/978-1-4939-9077-1_3.
Lenz, M.O., Sinclair, H.G., Savell, A., Clegg, J.H., Brown, A.C.N., Davis, D.M., et al., 2014. 3-D stimulated emission depletion microscopy with programmable aberration correction. J. Biophotonics 7, 29–36. https://doi.org/10.1002/jbio.201300041.
Levet, F., Tønnesen, J., Nägerl, U.V., Sibarita, J.-B., 2020. SpineJ: a software tool for quantitative analysis of nanoscale spine morphology. Methods 174, 49–55. https://doi.org/10.1016/j.ymeth.2020.01.020.
Lin, R., Clowsley, A.H., Lutz, T., Baddeley, D., Soeller, C., 2020. 3D super-resolution microscopy performance and quantitative analysis assessment using DNA-PAINT and DNA origami test samples. Methods 174, 56–71. https://doi.org/10.1016/j.ymeth.2019.05.018.
Los, G.V., Encell, L.P., McDougall, M.G., Hartzell, D.D., Karassina, N., Zimprich, C., et al., 2008. HaloTag: a novel protein labeling technology for cell imaging and protein analysis. ACS Chem. Biol. 3, 373–382. https://doi.org/10.1021/cb800025k.
Lu, C.-H., Tang, W.-C., Liu, Y.-T., Chang, S.-W., Wu, F.C.M., Chen, C.-Y., et al., 2019. Lightsheet localization microscopy enables fast, large-scale, and three-dimensional super-resolution imaging. Commun. Biol. 2, 1–10. https://doi.org/10.1038/s42003-019-0403-9.
Manley, S., Gillette, J.M., Patterson, G.H., Shroff, H., Hess, H.F., Betzig, E., et al., 2008. High-density mapping of single-molecule trajectories with photoactivated localization microscopy. Nat. Methods 5, 155–157. https://doi.org/10.1038/nmeth.1176.
Masch, J.-M., Steffens, H., Fischer, J., Engelhardt, J., Hubrich, J., Keller-Findeisen, J., et al., 2018. Robust nanoscopy of a synaptic protein in living mice by organic-fluorophore labeling. Proc. Natl. Acad. Sci. 115, E8047–E8056. https://doi.org/10.1073/pnas.1807104115.
Matsuzaki, M., Honkura, N., Ellis-Davies, G.C.R., Kasai, H., 2004. Structural basis of long-term potentiation in single dendritic spines. Nature 429, 761–766. https://doi.org/10.1038/nature02617.
Mishchenko, Y., Hu, T., Spacek, J., Mendenhall, J., Harris, K.M., Chklovskii, D.B., 2010. Ultrastructural analysis of hippocampal neuropil from the connectomics perspective. Neuron 67, 1009–1020. https://doi.org/10.1016/j.neuron.2010.08.014.
Möckl, L., Moerner, W.E., 2020. Super-resolution microscopy with single molecules in biology and beyond-essentials, current trends, and future challenges. J. Am. Chem. Soc. 142, 17828–17844. https://doi.org/10.1021/jacs.0c08178.
Mohapatra, N., Tønnesen, J., Vlachos, A., Kuner, T., Deller, T., Nägerl, U.V., et al., 2016. Spines slow down dendritic chloride diffusion and affect short-term ionic plasticity of GABAergic inhibition. Sci. Rep. 6, 23196. https://doi.org/10.1038/srep23196.
Nägerl, U.V., Willig, K.I., Hein, B., Hell, S.W., Bonhoeffer, T., 2008. Live-cell imaging of dendritic spines by STED microscopy. Proc. Natl. Acad. Sci. U. S. A. 105, 18982–18987. https://doi.org/10.1073/pnas.0810028105.
Neef, J., Urban, N.T., Ohn, T.-L., Frank, T., Jean, P., Hell, S.W., et al., 2018. Quantitative optical nanophysiology of Ca 2+ signaling at inner hair cell active zones. Nat. Commun. 9, 290. https://doi.org/10.1038/s41467-017-02612-y.
Osseforth, C., Moffitt, J.R., Schermelleh, L., Michaelis, J., 2014. Simultaneous dual-color 3D STED microscopy. Opt. Express 22, 7028–7039. https://doi.org/10.1364/OE.22.007028.
Pellett, P.A., Sun, X., Gould, T.J., Rothman, J.E., Xu, M.-Q., Corrêa, I.R., et al., 2011. Two-color STED microscopy in living cells. Biomed. Opt. Express 2, 2364–2371. https://doi.org/10.1364/BOE.2.002364.
Pfeiffer, T., Poll, S., Bancelin, S., Angibaud, J., Inavalli, V.K., Keppler, K., et al., 2018. Chronic 2P-STED imaging reveals high turnover of dendritic spines in the hippocampus in vivo. eLife 7. https://doi.org/10.7554/eLife.34700.
Power, R.M., Huisken, J., 2017. A guide to light-sheet fluorescence microscopy for multiscale imaging. Nat. Methods 14, 360–373. https://doi.org/10.1038/nmeth.4224.

Rust, M.J., Bates, M., Zhuang, X., 2006. Sub-diffraction-limit imaging by stochastic optical reconstruction microscopy (STORM). Nat. Methods 3, 793–795. https://doi.org/10.1038/nmeth929.

Sahl, S.J., Hell, S.W., 2019. High-resolution 3D light microscopy with STED and RESOLFT. In: Bille, J.F. (Ed.), High Resolution Imaging in Microscopy and Ophthalmology: New Frontiers in Biomedical Optics. Springer International Publishing, Cham, pp. 3–32. https://doi.org/10.1007/978-3-030-16638-0_1.

Sahl, S.J., Balzarotti, F., Keller-Findeisen, J., Leutenegger, M., Westphal, V., Egner, A., et al., 2016. Comment on "Extended-resolution structured illumination imaging of endocytic and cytoskeletal dynamics". Science 352, 527. https://doi.org/10.1126/science.aad7983.

Sasaki, T., Matsuki, N., Ikegaya, Y., 2011. Action-potential modulation during axonal conduction. Science 331, 599–601. https://doi.org/10.1126/science.1197598.

Schermelleh, L., Ferrand, A., Huser, T., Eggeling, C., Sauer, M., Biehlmaier, O., et al., 2019. Super-resolution microscopy demystified. Nat. Cell Biol. 21, 72–84. https://doi.org/10.1038/s41556-018-0251-8.

Schmied, J.J., Raab, M., Forthmann, C., Pibiri, E., Wünsch, B., Dammeyer, T., et al., 2014. DNA origami–based standards for quantitative fluorescence microscopy. Nat. Protoc. 9, 1367–1391. https://doi.org/10.1038/nprot.2014.079.

Soria, F.N., Miguelez, C., Peñagarikano, O., Tønnesen, J., 2020a. Current techniques for investigating the brain extracellular space. Front. Neurosci. 14 https://doi.org/10.3389/fnins.2020.570750.

Soria, F.N., Paviolo, C., Doudnikoff, E., Arotcarena, M.-L., Lee, A., Danné, N., et al., 2020b. Synucleinopathy alters nanoscale organization and diffusion in the brain extracellular space through hyaluronan remodeling. Nat. Commun. 11, 3440. https://doi.org/10.1038/s41467-020-17328-9.

Stahlberg, M.A., Ramakrishnan, C., Willig, K.I., Boyden, E.S., Deisseroth, K., Dean, C., 2019. Investigating the feasibility of channelrhodopsin variants for nanoscale optogenetics. Neurophotonics 6, 015007. https://doi.org/10.1117/1.NPh.6.1.015007.

Steffens, H., Wegner, W., Willig, K.I., 2020. In vivo STED microscopy: a roadmap to nanoscale imaging in the living mouse. Methods 174, 42–48. https://doi.org/10.1016/j.ymeth.2019.05.020.

Steshenko, O., Andrade, D.M., Honigmann, A., Mueller, V., Schneider, F., Sezgin, E., et al., 2016. Reorganization of lipid diffusion by myelin basic protein as revealed by STED nanoscopy. Biophys. J. 110, 2441–2450.

Takasaki, K., Sabatini, B.L., 2014. Super-resolution 2-photon microscopy reveals that the morphology of each dendritic spine correlates with diffusive but not synaptic properties. Front. Neuroanat. 8 https://doi.org/10.3389/fnana.2014.00029.

Takasaki, K.T., Ding, J.B., Sabatini, B.L., 2013. Live-cell superresolution imaging by pulsed STED two-photon excitation microscopy. Biophys. J. 104, 770–777. https://doi.org/10.1016/j.bpj.2012.12.053.

Tamada, H., Blanc, J., Korogod, N., Petersen, C.C., Knott, G.W., 2020. Ultrastructural comparison of dendritic spine morphology preserved with cryo and chemical fixation. eLife 9, e56384. https://doi.org/10.7554/eLife.56384.

Tanaka, J.-I., Horiike, Y., Matsuzaki, M., Miyazaki, T., Ellis-Davies, G.C.R., Kasai, H., 2008. Protein synthesis and neurotrophin-dependent structural plasticity of single dendritic spines. Science 319, 1683–1687. https://doi.org/10.1126/science.1152864.

Testa, I., Urban, N.T., Jakobs, S., Eggeling, C., Willig, K.I., Hell, S.W., 2012. Nanoscopy of living brain slices with low light levels. Neuron 75, 992–1000. https://doi.org/10.1016/j.neuron.2012.07.028.

Tønnesen, J., Nagerl, U.V., 2013. Superresolution imaging for neuroscience. Exp. Neurol. 242 https://doi.org/10.1016/j.expneurol.2012.10.004.

Tønnesen, J., Nagerl, U.V., 2013. Two-color STED imaging of synapses in living brain slices. Methods Mol. Biol. 950, 65–80. https://doi.org/10.1007/978-1-62703-137-0_5.

Tønnesen, J., Nägerl, U.V., 2016. Dendritic spines as tunable regulators of synaptic signals. Front. Psychiatry 7, 101. https://doi.org/10.3389/fpsyt.2016.00101.

Tønnesen, J., Nadrigny, F., Willig, K.I., Wedlich-Soldner, R., Nagerl, U.V., 2011. Two-color STED microscopy of living synapses using a single laser-beam pair. Biophys. J. 101 https://doi.org/10.1016/j.bpj.2011.10.011.

Tønnesen, J., Katona, G., Rózsa, B., Nägerl, U.V., 2014. Spine neck plasticity regulates compartmentalization of synapses. Nat. Neurosci. 17, 678–685.

Tønnesen, J., Inavalli, V.V.G.K., Nägerl, U.V., 2018. Super-resolution imaging of the extracellular space in living brain tissue. Cell 172, 1108–1121.e15. https://doi.org/10.1016/j.cell.2018.02.007.

Tortarolo, G., Castello, M., Diaspro, A., Koho, S., Vicidomini, G., 2018. Evaluating image resolution in stimulated emission depletion microscopy. Optica 5, 32–35. https://doi.org/10.1364/OPTICA.5.000032.

Turcotte, R., Liang, Y., Tanimoto, M., Zhang, Q., Li, Z., Koyama, M., et al., 2019. Dynamic super-resolution structured illumination imaging in the living brain. Proc. Natl. Acad. Sci. 116, 9586–9591. https://doi.org/10.1073/pnas.1819965116.

Urban, N.T., Willig, K.I., Hell, S.W., Nägerl, U.V., 2011. STED nanoscopy of actin dynamics in synapses deep inside living brain slices. Biophys. J. 101, 1277–1284. https://doi.org/10.1016/j.bpj.2011.07.027.

Velasco, M.G.M., Velasco, M.G.M., Zhang, M., Zhang, M., Antonello, J., Yuan, P., et al., 2021. 3D super-resolution deep-tissue imaging in living mice. Optica 8, 442–450. https://doi.org/10.1364/OPTICA.416841.

Watanabe, S., Punge, A., Hollopeter, G., Willig, K.I., Hobson, R.J., Davis, M.W., et al., 2011. Protein localization in electron micrographs using fluorescence nanoscopy. Nat. Methods 8, 80–84. https://doi.org/10.1038/nmeth.1537.

Wegner, W., Ilgen, P., Gregor, C., van Dort, J., Mott, A.C., Steffens, H., et al., 2017. In vivo mouse and live cell STED microscopy of neuronal actin plasticity using far-red emitting fluorescent proteins. Sci. Rep. 7, 11781. https://doi.org/10.1038/s41598-017-11827-4.

Wegner, W., Mott, A.C., Grant, S.G.N., Steffens, H., Willig, K.I., 2018. In vivo STED microscopy visualizes PSD95 sub-structures and morphological changes over several hours in the mouse visual cortex. Sci. Rep. 8, 219. https://doi.org/10.1038/s41598-017-18640-z.

Westphal, V., Rizzoli, S.O., Lauterbach, M.A., Kamin, D., Jahn, R., Hell, S.W., 2008. Video-rate far-field optical nanoscopy dissects synaptic vesicle movement. Science 320, 246–249. https://doi.org/10.1126/science.1154228.

Wildanger, D., Medda, R., Kastrup, L., Hell, S.W., 2009. A compact STED microscope providing 3D nanoscale resolution. J. Microsc. 236, 35–43. https://doi.org/10.1111/j.1365-2818.2009.03188.x.

Willig, K.I., Harke, B., Medda, R., Hell, S.W., 2007. STED microscopy with continuous wave beams. Nat. Methods 4, 915–918. https://doi.org/10.1038/nmeth1108.

Willig, K.I., Kellner, R.R., Medda, R., Hein, B., Jakobs, S., Hell, S.W., 2006. Nanoscale resolution in GFP-based microscopy. Nat. Methods 3, 721–723. https://doi.org/10.1038/nmeth922.

Willig, K.I., Stiel, A.C., Brakemann, T., Jakobs, S., Hell, S.W., 2011. Dual-label STED nanoscopy of living cells using Photochromism. Nano Lett. 11, 3970–3973. https://doi.org/10.1021/nl202290w.

Wilson, C.J., 1984. Passive cable properties of dendritic spines and spiny neurons. J. Neurosci. 4, 281–297. https://doi.org/10.1523/JNEUROSCI.04-01-00281.1984.

Xie, L., Kang, H., Xu, Q., Chen, M.J., Liao, Y., Thiyagarajan, M., et al., 2013. Sleep drives metabolite clearance from the adult brain. Science 342. https://doi.org/10.1126/science.1241224.

Xu, K., Zhong, G., Zhuang, X., 2013. Actin, spectrin, and associated proteins form a periodic cytoskeletal structure in axons. Science 339, 452–456. https://doi.org/10.1126/science.1232251.